Dispersion on kriged hydraulic conductivity fields

Olaf A. Cirpka and Wolfgang Nowak

Institut für Wasserbau, Universität Stuttgart, Stuttgart, Germany

Received 10 April 2001; revised 31 January 2002; accepted 12 April 2002; published 5 February 2003.

[1] Geostatistical interpolation of log conductivity measurements leads to velocity fields lacking small-scale variability whereas large-scale features are covered well. The unresolved, small-scale velocity fluctuations cause underestimation of macrodispersion, dilution, and mixing in subsequent transport calculations. The same holds when the best linear unbiased estimate of geostatistical inverse methods is used in flow and transport simulations. Considering a regular grid of measurement points, we approximate the lack of dispersion, to which we refer as correction dispersion, by applying first-order theory to the conditional covariance of the kriged log conductivity field. The nonstationarity of the conditional covariance is removed by averaging it over space. We distinguish between macrodispersion, describing the rate of change in the second spatial moments of a large plume, and effective dispersion of a plume introduced as a point source, parameterizing dilution and mixing. Depending on the objective, we either add a correction macrodispersion tensor or a correction effective dispersion tensor to the true local dispersion tensor in transport calculations on the smoothed log conductivity field. The numerical application to a two-dimensional periodic domain shows excellent agreement in the one- and two-particle moments between simulations on the highly resolved field and those on the interpolated one using corrected values for the local dispersion coefficients. *INDEX TERMS:* 1829 Hydrology: Groundwater hydrology; 1832 Hydrology: Groundwater transport; 1869 Hydrology: Stochastic processes; *KEYWORDS:* solute dispersion, kriging, conditional covariance, spectral filter

Citation: Cirpka, O. A., and W. Nowak, Dispersion on kriged hydraulic conductivity fields, *Water Resour. Res.*, *39*(2), 1027, doi:10.1029/2001WR000598, 2003.

1. Introduction

[2] In the last two decades, the impact of heterogeneity on solute transport in natural formations has gained high attention. The stochastic description of (log-)hydraulic conductivity has been proven an adequate framework for handling spatial variability and uncertainty. Based on second-order statistics, that is, the geometric mean of the hydraulic conductivity and a covariance model of the log conductivity fluctuations, closed-form expressions have been developed for macrodispersion, i.e., the spreading of a large solute plume [*Gelhar and Axness*, 1983; *Neuman et al.*, 1987; *Dagan*, 1988] and, more recently, effective dispersion of smaller plumes [*Rajaram and Gelhar*, 1993; *Attinger et al.*, 1999; *Dentz et al.*, 2000], and the concentration variance [*Fiori and Dagan*, 2000]. These studies have deepened our understanding of solute transport in heterogeneous domains. Applying the resulting expressions to real cases, however, puts us into an ironic situation. Although a considerably high number of measurements is needed to retrieve the statistical parameters required by the methods described in the studies mentioned above, the measurements themselves are dismissed altogether and only the statistical parameters are used.

[3] A related field of stochastic hydrology deals with inferring the distribution of hydraulic conductivity by interpolating hydraulic-conductivity measurements or inversing hydraulic-head and concentration measurements [see, e.g., *McLaughlin and Townley*, 1996; *Zimmerman et al.*, 1998]. In the geostatistical framework, interpolation and inverse modeling is identical to evaluating the best linear unbiased estimate (BLUE), or conditional mean, of the log-hydraulic conductivity distribution. It is well known that the distribution of the BLUE is smoother than the true conductivity field. In particular, it is smoother than described by the prior covariance model used in the conditioning procedure. Consider the covariance function $R_{YY}(\mathbf{x}, \mathbf{x} + \mathbf{h})$ of log conductivity fluctuations on the fully resolved field. Then the fluctuations on the kriged field are given by the covariance function $R_k(\mathbf{x}, \mathbf{x} + \mathbf{h})$ which is $R_{YY}(\mathbf{x}, \mathbf{x} + \mathbf{h})$ minus the conditional covariance $R_c(\mathbf{x}, \mathbf{x} + \mathbf{h})$:

$$R_k(\mathbf{x}, \mathbf{x}+\mathbf{h}) = R_{YY}(\mathbf{x}, \mathbf{x}+\mathbf{h}) - R_c(\mathbf{x}, \mathbf{x}+\mathbf{h}) \qquad (1)$$

Note that $R_c(\mathbf{x}, \mathbf{x} + \mathbf{h})$ depends on the exact location even if $R_{YY}(\mathbf{x}, \mathbf{x} + \mathbf{h})$ is stationary. Figures 1a and 1e show a fully resolved log conductivity field $Y(\mathbf{x})$ and its approximation by kriging using point values taken from the original field on a regular grid of observation points. After kriging, small-scale structures have been smoothed out.

[4] In a thought experiment, we imply a mean head-gradient into the x_1 direction. Then the fluctuations of the log conductivity field cause those of the velocity field. By first-order theory, we can relate the covariance of log

0043-1397/03/2001WR000598$09.00

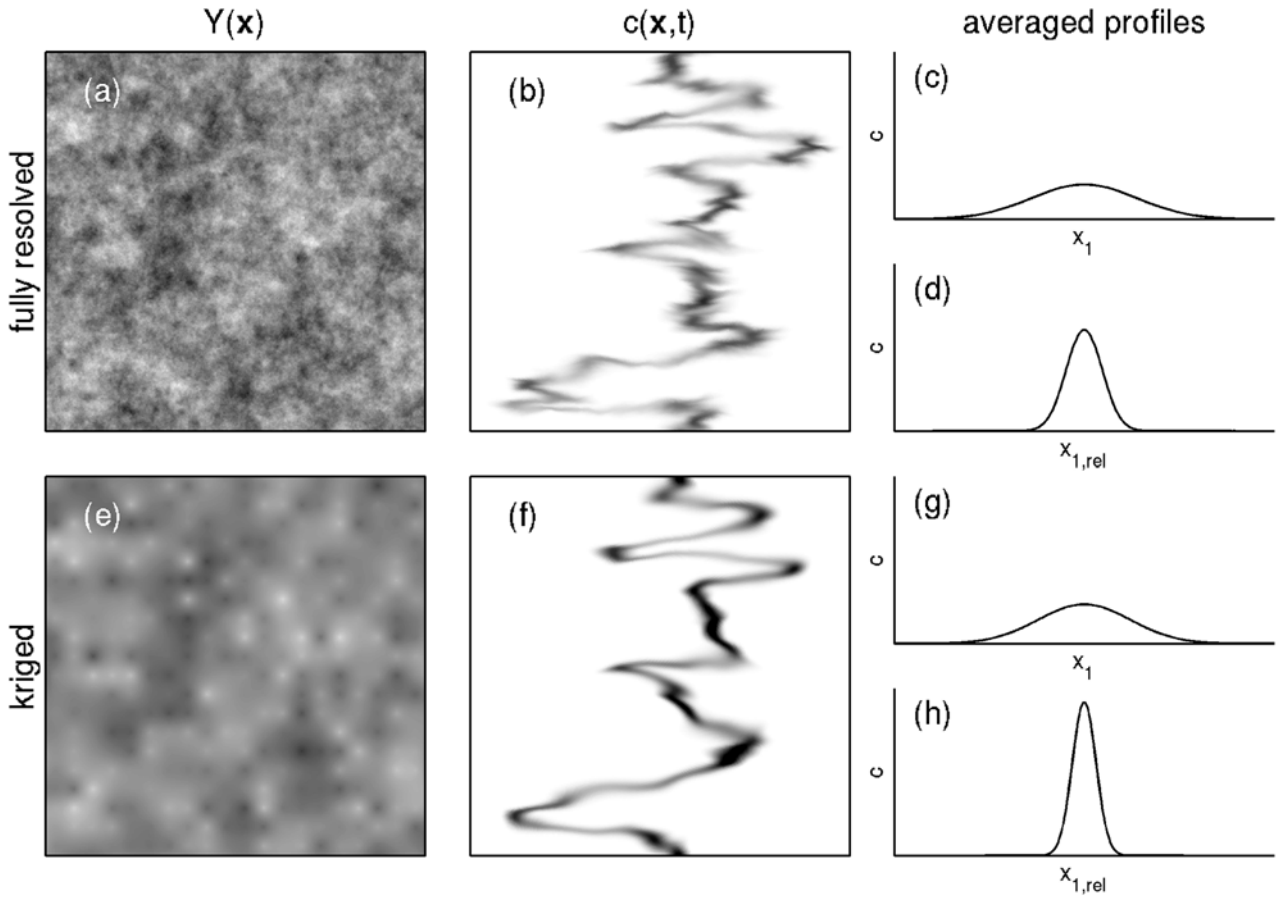

Figure 1. Effect of geostatistical interpolation on solute transport. Figures 1a and 1e: fully resolved and interpolated log conductivity fields. Figures 1b and 1f: corresponding concentration distribution for macroscopically uniform flow due to a line source injection. Figures 1c and 1g: profiles of concentrations averaged over the cross section of the domain. Figures 1d and 1h: averaged concentration profiles in which the longitudinal coordinate has been corrected for the center of gravity for each x_2 value prior to averaging.

conductivity to that of velocity fluctuations about the overall mean velocity, at least under stationary conditions [*Bakr et al.*, 1978; *Gelhar and Axness*, 1983]. We continue our thought experiment by introducing a conservative tracer as a line source into the heterogeneous domain. The resulting concentration distributions after a certain period of time are shown in Figure 1b for the fully resolved field and Figure 1f for the kriged field. Because the interpolated log conductivity field is smoother than the fully resolved one, the corresponding concentration distribution shows smaller fluctuations and is more peaked.

[5] For comparison, we use two different averaging procedures. In the evaluation of longitudinal macrodispersion, we average the concentration over the cross section perpendicular to the direction of mean flow. The resulting concentration profiles are illustrated in Figure 1c for the fully resolved log conductivity field and Figure 1g for the kriged one. Then, we define the macrodispersion coefficient by half the rate of change of the second central moment of these profiles. Longitudinal macrodispersion is dominated by the fluctuating mean position of the line-shaped plume. If we want to quantify how wide, in average, the plume is at a given x_2 value, macrodispersion gives a too large value. A more expedient quantity for the latter task is the longitudinal effective dispersion coefficient. Here, we first subtract the center of gravity for each x_2 value from the longitudinal coordinate x_1, and subsequently perform the averaging over the cross section. The resulting concentration profiles on the fully resolved and interpolated log conductivity fields are shown in Figures 1d and 1h, respectively. In analogy to macrodispersion, the effective dispersion coefficient is half the rate of change of the second central moment of these profiles. Obviously, the profiles in Figures 1d and 1h are more peaked than their counterpart in Figures 1c and 1g; that is, the effective dispersion coefficients are considerably smaller than the macrodispersion coefficients. Macrodispersion is a parameter of overall spreading, whereas effective dispersion is a measure of dilution. Given a stationary velocity field, we can predict both macrodispersion and effective dispersion by first-order theory [*Gelhar and Axness*, 1983; *Neuman et al.*, 1987; *Dagan*, 1988; *Dentz et al.*, 2000; *Fiori and Dagan*, 2000].

[6] If we compare Figure 1c with Figure 1g and Figure 1d with Figure 1h, we observe that simulating transport on a conductivity field retrieved from kriging leads to an underestimation of dispersion, namely of effective dispersion. Consider $\mathbf{D}^e(t)$ the time-dependent effective dispersion tensor on the fully resolved field and $\tilde{\mathbf{D}}^e(t)$ the effective

dispersion tensor resulting from calculations on the kriged field. Then, we suggest to increase the local dispersion tensor in simulations on interpolated log conductivity fields by a correction effective dispersion tensor $\mathbf{D}_c^e(t)$ in order to meet the dispersive behavior of the fully resolved fields:

$$\mathbf{D}_c^e(t) = \mathbf{D}^e(t) - \tilde{\mathbf{D}}^e(t) \tag{2}$$

If we want to meet the macrodispersive behavior, we will need a correction macrodispersion tensor $\mathbf{D}_c^*(t)$ which differs from $\mathbf{D}_c^e(t)$. Adopting and extending the approach of *Rubin et al.* [1999] derived for block-wise averaged log conductivity values, we can estimate $\mathbf{D}_c^*(t)$ and $\mathbf{D}_c^e(t)$ from the conditional covariance function, describing the variability of log conductivity that is lost in the kriging procedure. Since we take volume averages in the evaluation of both types of dispersion, we can derive the dispersion coefficients from the velocity fluctuations about the same overall uniform mean velocity. We remove the nonstationarity of the conditional covariance function $R_c(\mathbf{x}, \mathbf{x} + \mathbf{h})$ of log conductivity by spatial averaging. Then, we can substitute the averaged conditional covariance function $\bar{R}_c(\mathbf{h})$ into the standard equations deriving the macrodispersion and effective dispersion coefficients in stationary fields, yielding expressions for the correction dispersion tensors.

[7] The paper is organized as follows. In section 2, we review the evaluation of the conditional covariance in kriging. Section 3 contains the expressions used for macrodispersion (section 3.1) and effective dispersion of a point source (section 3.2) as well as the approach to account for the smoothing of the conductivity field by geostatistical interpolation (section 3.3). In section 4, we apply the approach to a spatially periodic two-dimensional domain.

2. Covariance of Kriged Log Conductivity Fields

[8] Consider the log conductivity field $Y(\mathbf{x}) = \ln(K(\mathbf{x}))$ a stationary random function characterized by its mean $\bar{Y}$ and covariance $R_{YY}(\mathbf{h})$:

$$\bar{Y} = \langle Y \rangle \neq f(\mathbf{x}) \tag{3}$$

$$R_{YY}(\mathbf{h}) = \langle (Y(\mathbf{x}) - \bar{Y})(Y(\mathbf{x}+\mathbf{h}) - \bar{Y}) \rangle \neq f(\mathbf{x}) \tag{4}$$

in which $\langle\ \rangle$ denotes the expected value operator, and $\mathbf{h}$ is the separation vector. The Fourier transform of the covariance function $R_{YY}(\mathbf{h})$ is the power spectral density function of the log conductivity fluctuations $S_{YY}(\mathbf{s})$:

$$S_{YY}(\mathbf{s}) = \frac{1}{(2\pi)^{d/2}} \int_{V_\infty} R_{YY}(\mathbf{h})\, \exp(i\,\mathbf{h}\cdot\mathbf{s}) d\mathbf{h} \tag{5}$$

in which $\mathbf{s}$ is the vector of wave numbers, d is the dimensionality of the domain, and i is the imaginary number.

[9] Consider the log conductivity Y to be exactly known at the n_m measurement locations $\hat{\mathbf{x}}_i$. The (generalized) covariance of the log conductivity is assumed known, whereas the mean value of Y must be estimated. Then, the estimate by ordinary kriging is the expected mean of the log conductivity field conditioned on the measurements. We formulate the interpolation by kriging in the function-estimate form [see, e.g., *Kitanidis*, 1996]:

$$\tilde{Y}(\mathbf{x}) = \hat{\beta} + \sum_{i=1}^{n_m} R_{YY}(\mathbf{x} - \hat{\mathbf{x}}_i)\xi_i \tag{6}$$

in which $\tilde{Y}(\mathbf{x})$ is the best linear unbiased estimate (BLUE) of the log conductivity at location $\mathbf{x}$, whereas $\hat{\beta}$ is the estimated overall mean, and ξ_i is a weighting factor of measurement i. These coefficients are determined by solving the kriging system:

$$\begin{bmatrix} \mathbf{R}_{\hat{Y}\hat{Y}} & \mathbf{u} \\ \mathbf{u}^T & 0 \end{bmatrix} \begin{bmatrix} \boldsymbol{\xi} \\ \hat{\beta} \end{bmatrix} = \begin{bmatrix} \hat{\mathbf{Y}} \\ 0 \end{bmatrix} \tag{7}$$

in which $\mathbf{R}_{\hat{Y}\hat{Y}}$ is the covariance matrix of the log conductivity at all measurement points, $\mathbf{u}$ is the vector of drift coefficients consisting of n_m entries of unity, and $\hat{\mathbf{Y}}$ is the vector of measured log-conductivities. *Kitanidis* [1996] gives the following analytical result for the conditional covariance $R_c(\mathbf{x}_1, \mathbf{x}_2)$:

$$\begin{aligned} R_c(\mathbf{x}_1, \mathbf{x}_2) = R_{YY}(\|\mathbf{x}_1 - \mathbf{x}_2\|) \\ - \Bigg(P_\beta + \sum_{j=1}^{n_m} \left(R_{YY}(\mathbf{x}_1, \hat{\mathbf{x}}_j) p_{j\beta} + p_{\beta j} R_{YY}(\hat{\mathbf{x}}_j, \mathbf{x}_2) \right. \\ \left. + \sum_{k=1}^{n_m} \left(R_{YY}(\mathbf{x}_1, \hat{\mathbf{x}}_j) P_{jk} R_{YY}(\hat{\mathbf{x}}_k, \mathbf{x}_2) \right) \right) \Bigg) \end{aligned} \tag{8}$$

in which coefficient P_{jk} is the j, kth entry of the $n_m \times n_m$ matrix $\mathbf{P}_{\hat{x}\hat{x}}$, $p_{j\beta}$ is the jth entry of the $n_m \times 1$ vector $\mathbf{p}_{\hat{x}\beta}$, and P_β is a scalar where $\mathbf{P}_{\hat{x}\hat{x}}$, $\mathbf{p}_{\hat{x}\beta}$ and P_β are taken from the inverse of the kriging matrix:

$$\begin{bmatrix} \mathbf{P}_{\hat{x}\hat{x}} & \mathbf{p}_{\hat{x}\beta} \\ \mathbf{p}_{\hat{x}\beta}^T & P_\beta \end{bmatrix} = \begin{bmatrix} \mathbf{R}_{\hat{Y}\hat{Y}} & \mathbf{u} \\ \mathbf{u}^T & 0 \end{bmatrix}^{-1} \tag{9}$$

[10] The conditional covariance $R_c(\mathbf{x}, \mathbf{x} + \mathbf{h})$ quantifies the variability of log conductivity unresolved by the kriging procedure, whereas $R_{YY}(\mathbf{h}) - R_c(\mathbf{x}, \mathbf{x} + \mathbf{h})$ describes the expected variability of the kriged field. For the case of zero separation, $\mathbf{h} = \mathbf{0}$, the conditional covariance $R_c(\mathbf{x}, \mathbf{x})$ is also known as estimation variance. The more dense the measurement points are, the more variability is captured in the kriged field, and the smaller $R_c(\mathbf{x}, \mathbf{x} + \mathbf{h})$ becomes. In principle, we can extend the analysis to include measurements of hydraulic heads or other dependent quantities. The corresponding cokriging equations are similar to the kriging equations given above.

[11] $R_c(\mathbf{x}, \mathbf{x} + \mathbf{h})$ depends not only on the separation vector $\mathbf{h}$ but also on the exact location $\mathbf{x}$, that is, $R_c(\mathbf{x}, \mathbf{x} + \mathbf{h})$ is nonstationary. The variance is fully recovered at the measurement points, whereas it is significantly smaller at the points with maximum distance to the next measurement locations. For the further analysis, we remove this nonstationarity by taking spatial averages of the filtered covariances. That is, although the filtered fields are nonstationary, we treat them like stationary ones. This allows us to use

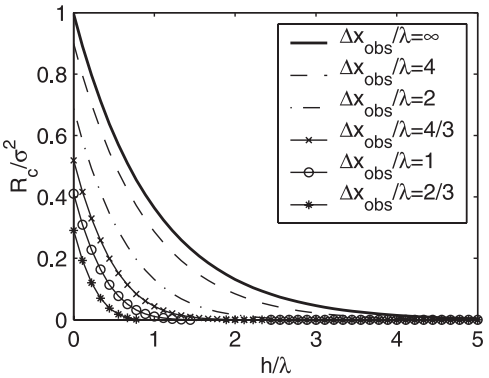

Figure 2. Spatially averaged conditional covariance $\bar{R}_c(h)$ for the exponential model with different spacings of observation points.

approaches for the evaluation of macrodispersion and effective dispersion on the kriged field that have been developed for stationary fields. Also, we assume a regular grid of measurement locations.

[12] In order to remove the nonstationary, we take the spatial average of $R_c(\mathbf{x}, \mathbf{x} + \mathbf{h})$:

$$\bar{R}_c(\mathbf{h}) = \lim_{L_1,L_2,L_3\to\infty} \frac{1}{L_1L_2L_3} \int_{-L_1/2}^{+L_1/2}\int_{-L_2/2}^{+L_2/2}\int_{-L_3/2}^{+L_3/2} \cdot R_c(\mathbf{x}, \mathbf{x}+\mathbf{h})\, dx_3\, dx_2\, dx_1 \tag{10}$$

[13] The evaluation of the actual conditional covariance matrix $R_c(\mathbf{x}_1, \mathbf{x}_2)$ by equation (8) can be tedious because $\mathbf{R}_c$ is a square matrix of the order of the number of points discretizing the domain. By contrast, $\bar{R}_c(\mathbf{h})$ is a vector of the same order and requires much less computational memory. In the appendix, we derive an efficient semianalytical method for the calculation of $\bar{R}_c(\mathbf{h})$ that circumvents the calculation of the actual conditional covariance matrix $R_c(\mathbf{x}_1, \mathbf{x}_2)$. Based on these expressions, Figure 2 shows the profile of the spatially averaged covariance function $\bar{R}_c(\mathbf{h})$ along the x_1-axis for the case of the two-dimensional isotropic exponential model of the unconditional covariance function. The wider the grid spacing, the closer is the conditional covariance to the unconditional. More dense observation points lead also to smaller integral scales.

3. Dispersion Coefficients

3.1. Macrodispersion

[14] The macrodispersion tensor is defined as the dispersion tensor needed to match the second central spatial moments of a very large plume in a heterogeneous domain when transport is described by the uniform advection-dispersion equation. In the Lagrangian framework, the normalized second central moments are expressed as variance of particle displacements $\langle \mathbf{X}'\mathbf{X}'^T \rangle$ taken from the ensemble of particles each introduced into a single realization of the random spatial field. Then, the time-dependent macrodispersion tensor $\mathbf{D}^*(t)$ is half the rate of change of $\langle \mathbf{X}'\mathbf{X}'^T \rangle$ [see, e.g., *Dagan*, 1984]. In the Eulerian framework, the macrodispersive flux is the flux due to local dispersion $-\mathbf{D}\nabla c$ plus the covariance of seepage velocity fluctuations and concentration fluctuations $\langle \mathbf{v}'c' \rangle$, again applying the ensemble average [see, e.g., *Gelhar and Axness*, 1983]. The full macrodispersion tensor is retrieved by applying unit concentration gradients in all principle directions of the system of coordinates. In stationary velocity fields with small log conductivity fluctuations, linear stochastic theory yields [*Gelhar and Axness*, 1983; *Neuman et al.*, 1987; *Dagan*, 1988]:

$$\mathbf{D}^*(t) = \frac{1}{2}\frac{\partial \langle \mathbf{X}'\mathbf{X}'^T \rangle}{\partial t} = \mathbf{D} + \frac{1}{(2\pi)^{d/2}} \int_{V_\infty} -\left(\mathbf{s}^T\mathbf{D}\mathbf{s} - i\mathbf{s}\cdot\bar{\mathbf{v}}\right) \cdot \frac{1-\exp(-t(i\mathbf{s}\cdot\bar{\mathbf{v}} + \mathbf{s}^T\mathbf{D}\mathbf{s}))}{(\mathbf{s}\cdot\bar{\mathbf{v}})^2 + (\mathbf{s}^T\mathbf{D}\mathbf{s})^2} \cdot \mathbf{S}_{\mathbf{vv}}(\mathbf{s})\, d\mathbf{s} \tag{11}$$

in which $\mathbf{X}$ is the one-particle displacement, $\mathbf{D}$ is the local dispersion tensor assumed uniform $\bar{\mathbf{v}}$ is the mean seepage velocity, t is time, and $\mathbf{S}_{\mathbf{vv}}(\mathbf{s})$ is the spectrum of all seepage-velocity components. For a uniform effective porosity θ and a uniform gradient of the mean head $-\mathbf{J}$, the spectrum of seepage-velocity components $\mathbf{S}_{\mathbf{vv}}(\mathbf{s})$ can be evaluated from that of log conductivity $S_{YY}(\mathbf{s})$ by [*Bakr et al.*, 1978; *Gelhar and Axness*, 1983]:

$$\mathbf{S}_{\mathbf{vv}}(\mathbf{s}) = \left(\mathbf{J} - \frac{\mathbf{s}\cdot\mathbf{J}}{s^2}\mathbf{s}\right)\left(\mathbf{J} - \frac{\mathbf{s}\cdot\mathbf{J}}{s^2}\mathbf{s}\right)^T \frac{K_g^2}{\theta^2} S_{YY}(\mathbf{s}) \tag{12}$$

in which $K_g = \exp(\bar{Y})$ is the geometric mean of the hydraulic conductivity K.

3.2. Effective Dispersion

[15] The macroscopic parameters derived through volume-averaging over a single realization and ensemble-averaging over an infinite number of realizations become identical at the limit of an infinite initial size of the plume. In all practical applications, however, the solute plumes are finite, and the second central moments of the ensemble-averaged concentration merge two types of information: the expected second central moments of the real plume and the uncertainty in predicting the center of mass [*Kitanidis*, 1988]. Half the rate of change of the expected second central moment of a plume with finite initial size is quantified by the effective dispersion tensor $\mathbf{D}^e(t, \mathbf{V}_0)$ which is a function of time and the initial volume of the plume $\mathbf{V}_0$ [*Rajaram and Gelhar*, 1993; *Attinger et al.*, 1999; *Dentz et al.*, 2000]. The smaller the initial size of the plume, the higher is the contribution of uncertainty in the plume location to ensemble-averaged macrodispersion. In the following, we consider the limit of a point-like injection, $\mathbf{V}_0 = \mathbf{0}$, for which the dispersion theories based on strictly advective transport predict zero effective dispersion. Accounting for local dispersion, the effective dispersion tensor is initially identical to the local dispersion tensor, grows over time since local transverse dispersion makes the plume sample increasingly more streamlines, and finally reaches the asymptotic macrodispersion tensor, although at very large times [*Attinger et al.*, 1999; *Dentz et al.*, 2000].

[16] The significance of $\mathbf{D}^e(t, \mathbf{0})$ reaches beyond the temporal development of spatial moments due to a point-like injection of a conservative tracer. It also quantifies the adjoint problem: For longitudinal effective dispersion, we inject the tracer as a pulse into a control plane perpendicular

to the direction of mean flow and quantify the average longitudinal spreading observed along single lines into the longitudinal direction (see Figure 1). For transverse effective dispersion, the injection-plane is parallel to the mean direction of flow, and we quantify average spreading along single lines normal to the injection plane. Therefore $\mathbf{D}^e(t, \mathbf{0})$ quantifies the overlapping of adjacent plumes that have been separate in the initial state. That is, $\mathbf{D}^e(t, \mathbf{0})$ is a measure of dispersive mixing. In calculations of mixing-controlled reactive transport, $\mathbf{D}^e(t, \mathbf{0})$ is the macroscopic dispersion parameter that guarantees the accurate mass balance, although the spatial moments of the reactive plumes will be underestimated.

[17] In the Lagrangian framework, the effective dispersion coefficients are evaluated by the two-particle moments of displacement: Conceptually, two particles are jointly introduced into each realization of the random field at the same location. Denote the displacement of the first particle by $\mathbf{X}_1(t)$, and that of the second by $\mathbf{X}_2(t)$. Then, the expression of the two-particle covariance by *Fiori and Dagan* [1999] can be reformulated to the following term for the difference between the macrodispersion tensor $\mathbf{D}^*(t)$ and the effective dispersion tensor $\mathbf{D}^e(t, \mathbf{0})$ in a stationary velocity field with zero initial volume:

$$\mathbf{D}^*(t) - \mathbf{D}^e(t,\mathbf{0}) = \frac{1}{2}\frac{\partial\langle \mathbf{X}_1'\mathbf{X}_2'^T\rangle}{\partial t} = \frac{1}{(2\pi)^{d/2}}\int_{V_\infty}\frac{\mathbf{s}^T\mathbf{D}\mathbf{s} - i\mathbf{s}\cdot\bar{\mathbf{v}}}{(\mathbf{s}\cdot\bar{\mathbf{v}})^2+(\mathbf{s}^T\mathbf{D}\mathbf{s})^2} \cdot \left(\exp\left(\left(i\mathbf{s}\cdot\bar{\mathbf{v}} - \mathbf{s}^T\mathbf{D}\mathbf{s}\right)t\right) - \exp\left(-2\mathbf{s}^T\mathbf{D}\mathbf{s}t\right)\right) \cdot \mathbf{S}_{\mathbf{vv}}(\mathbf{s})d\mathbf{s} \quad (13)$$

Dentz et al. [2000] derived equation (13) in an Eulerian framework; their analysis also included the effects of a spatially varying retardation factor. The effective dispersion tensor $\mathbf{D}^e(t, \mathbf{0})$ is given by subtracting equation (13) from equation (11). For small local dispersion values and early times, equations (11) and (13) hardly differ. This makes $\mathbf{D}^e(t, \mathbf{0})$ sensitive to small errors caused by higher-order effects not accounted for in the derivations of equations (11) and (13).

3.3. Correcting the Smoothing Effect of Kriging

[18] The expressions for macrodispersion and effective dispersion, equations (11) and (13), are based on second-order statistics of the unconditional log conductivity field. When we use kriged log conductivity fields for transport calculations, only a fraction of the true variability is resolved. The missing variability is quantified by $R_c(\mathbf{x}_1, \mathbf{x}_2)$ given by equation (8).

[19] If we wanted to quantify the uncertainty in tagging a particle in the kriged field starting at a definite point, we had to follow a rigorous nonstationary approach. On the kriged field, the BLUE of the velocity depends on the actual position. Also, the velocity fluctuation about the BLUE are nonstationary. For this purpose, *Rubin* [1991] developed a method assuming strictly advective transport in which the velocity covariance was sampled along the mean conditional trajectory. A more rigorous framework for the trajectory uncertainty in stochastic fields with nonstationary mean is given by *Indelman and Rubin* [1996] [see also *Sun and Zhang*, 2000]. As the BLUE of the velocity does not exhibit a simple trend but irregular fluctuations about an overall mean, closed-form expressions can not be derived.

[20] Here, we consider a simpler problem where we inject the tracer by an injection plane and analyze the average behavior of all particles. The fraction of dispersion that is recovered by calculations on the kriged field can be derived from the velocity fluctuations of the BLUE about the uniform mean velocity. We further simplify the problem by using the spatially averaged conditional covariance $\bar{R}_c(\mathbf{h})$ of log conductivity rather than the nonstationary $R_c(\mathbf{x}, \mathbf{x} + \mathbf{h})$. Now, the contributions to the fully resolved variability $R_{YY}(\mathbf{h})$ act additive on the dispersion coefficients. This follows from the definition of the Fourier transform, equation (5), and the linear relationships between the spectra of log conductivity and velocity components, equation (12), as well as between the velocity spectrum and the dispersion coefficients, equations (11) and (13). That is, we can split $R_{YY}(\mathbf{h})$ into the part covered by the kriged field, $R_{YY}(\mathbf{h}) - \bar{R}_c(\mathbf{h})$, and the unresolved part, $\bar{R}_c(\mathbf{h})$. We evaluate the effect of each component on $\mathbf{D}^*(t)$ and $\mathbf{D}^e(t, \mathbf{0})$ separately by the equations mentioned above, and finally sum up all contributions to dispersion. While the contribution of $R_{YY}(\mathbf{h}) - \bar{R}_c(\mathbf{h})$ to dispersion is automatically met by transport calculations on the kriged field, we must parameterize the contribution of $\bar{R}_c(\mathbf{h})$.

[21] We denote the macrodispersion tensor related to the fully resolved field by $\mathbf{D}^*(t)$ and that of the smoothed field by $\tilde{\mathbf{D}}^*(t)$. Then the difference $\mathbf{D}_c^*(t) = \mathbf{D}^*(t) - \tilde{\mathbf{D}}^*(t)$, to which we refer as correction macrodispersion tensor, describes the spreading of the plume that has been lost through smoothing of the log conductivity field. Analogously, we denote the effective dispersion tensor on the fully resolved field by $\mathbf{D}^e(t, \mathbf{0})$ and that on the smoothed field by $\tilde{\mathbf{D}}^e(t, \mathbf{0})$, and the difference $\mathbf{D}_c^e(t, \mathbf{0}) = \mathbf{D}^e(t, \mathbf{0}) - \tilde{\mathbf{D}}^e(t, \mathbf{0})$, to which we refer as correction effective dispersion tensor, describes the amount of mixing that has been lost through smoothing.

[22] Whenever we apply kriging, or cokriging, we assume a certain covariance function of the true field $R_{YY}(\mathbf{h})$. Provided a sufficient number of measurements, the validity of the assumed covariance function can be tested by cross-evaluation techniques such as the method of orthonormal residuals [*Kitanidis*, 1991]. This allows to calculate the expected macrodispersion and effective tensors on the true field $\mathbf{D}^*(t)$ and $\mathbf{D}^e(t, \mathbf{0})$, respectively. Through equations (8) and (10), we also know the conditional covariance of the log conductivity field $R_c(\mathbf{x}_1, \mathbf{x}_2)$ and its stationary simplification $\bar{R}_c(\mathbf{h})$. Substituting $\bar{R}_c(\mathbf{h})$ into equation (5) results in the averaged conditional spectrum $\bar{S}_c(\mathbf{h})$ which yields, through equations (11)–(13), the correction macrodispersion and effective dispersion coefficients $\mathbf{D}_c^*(t)$ and $\mathbf{D}_c^e(t, \mathbf{0})$, respectively.

[23] Adopting and extending the idea of *Rubin et al.* [1999], we may add $\mathbf{D}_c^*(t)$ and $\mathbf{D}_c^e(t, \mathbf{0})$, respectively, to the local dispersion tensor $\mathbf{D}$ in transport calculations on the smoothed grid in order to achieve the correct spreading or mixing behavior of the plume. That is, depending on the objective, we use two different "local" dispersion tensors in the calculations on the smoothed grid. If the overall spreading is of primary concern, we use $\mathbf{D} + \mathbf{D}_c^*(t)$, whereas $\mathbf{D} + \mathbf{D}_c^e(t, \mathbf{0})$ is used when mixing is more important. The correction macrodispersion tensor $\mathbf{D}_c^*(t)$ and the correction effective dispersion tensor $\mathbf{D}_c^e(t, \mathbf{0})$ depend on the spacing of

observation points and the model of the fully resolved log conductivity field. By considering the specifics of smoothing through kriging, our approach differs from that of *Rubin et al.* [1999] who simplified the effects of block-averaging by cutting off the log conductivity spectrum at the Nyquist wave number. Also, effective dispersion was not considered in the latter study.

[24] A complication in applying the approach arises from the impact of local dispersion on macrodispersion and effective dispersion. Consider coordinate $\mathbf{x}_1$ in the direction of mean flow. Then, choosing $\mathbf{D} + \mathbf{D}_c^*(t)$ rather than $\mathbf{D}$ as "local" dispersion tensor on the smoothed grid has two effects on macrodispersion. The primary effect is by the component D_{11} which is additive to longitudinal macrodispersion. By increasing D_{11}, we correct exactly for the kriging-induced smoothing. However, we also alter D_{22} in order to meet the transverse macrodispersion behavior, which has a dampening effect on longitudinal macrodispersion so that the correction will no more be exact. Considering realistic parameter values, fortunately, the impact of local transverse dispersion on longitudinal macrodispersion is fairly small [*Fiori*, 1996], and so is the error introduced by using the full correction macrodispersion tensor rather than its longitudinal component only. On the contrary, local dispersion has a major impact on effective dispersion. By choosing a "local" dispersion tensor of $\mathbf{D} + \mathbf{D}_c^e(t, \mathbf{0})$ rather than $\mathbf{D}$, we may increase longitudinal and transverse mixing significantly via both the D_{11}- and D_{22}-components. In the following application, we will add different components of the correction dispersion tensors $\mathbf{D}_c^*(t)$ and $\mathbf{D}_c^e(t, \mathbf{0})$ to the local dispersion tensor to evaluate the cross effects between longitudinal and transverse components.

4. Application to a Two-Dimensional Periodic Domain

4.1. Numerical Methods

[25] All equations in the preceding sections were formulated for stationary media and therefore infinite domains. An expedient approximation of stationary media are periodic ones where the log conductivity values are exactly repeated at distances that are integer multiples of L_1, L_2, and L_3 in the directions x_1, x_2, and x_3, respectively [*Kitanidis*, 1992]. Then, the log conductivity field is fully described by a single unit cell of size $L_1 \times L_2 \times L_3$. Nonetheless, the periodic domain is infinite. In periodic media, the Fourier integral of equation (5) is replaced by the corresponding Fourier series which is truncated in the discrete Fourier transform method. Because of the computational effort, we restrict the following example to the two-dimensional case.

[26] We generate 50 periodic fields of 1000×500 cells by a spectral approach similar to that of *Dykaar and Kitanidis* [1992] using an isotropic exponential covariance function:

$$R_{YY}(\mathbf{h}) = \exp\left(-\frac{\|\mathbf{h}'\|}{\lambda}\right) \tag{14}$$

in which λ is the correlation length, and $\mathbf{h}'$ is a separation vector modified to account for periodicity:

$$h_i' = \min(h_i, L_i - h_i) \tag{15}$$

Table 1. Parameters of the Test Case

Parameter	Value
Dimensions of domain	$\frac{L_1}{\lambda} = 50,\ \frac{L_2}{\lambda} = 25$
Spatial discretization	$\frac{\Delta x_1}{\lambda} = \frac{\Delta x_2}{\lambda} = 0.05$
Spacing of measurements	$\frac{\Delta x_{1,obs}}{\lambda} = \frac{\Delta x_{2,obs}}{\lambda} = 1.25$
Covariance model	isotropic exponential
Variance of Y	$\sigma_Y^2 = 0.25$
Local dispersion	scalar
Péclet number	$Pe = \frac{K_g J \lambda}{\theta D} = 500$

The parameters of the fields are given in Table 1. Equation (14) describes the covariance function within a single unit cell. For distance components larger than $L_1 \times L_2$, periodicity requires:

$$R_{YY}([h_1 + kL_1, h_2 + \ell L_2]) = R_{YY}([h_1, h_2]) \forall k, \ell \in [\ldots, -2, -1, 0, 1, 2, \ldots] \tag{16}$$

For each realization, we "take measurements" on a regular grid of observation points with a spacing of $\Delta x_{obs} = 1.25\lambda$, that is, we pick 40×20 evenly spaced log conductivity values from the fully resolved distributions. For each set of "measurements", we perform interpolation by ordinary kriging using the original covariance function that accounts for the periodicity. Therefore the 50 interpolated log conductivity fields are also periodic.

[27] Assuming a mean head-gradient $\mathbf{J} = [-J, 0]$ in the x_1 direction, the hydraulic heads ϕ in the infinite, periodic domain exhibit a linear trend with periodic fluctuations. Except for a constant, the hydraulic head field is fully described by the hydraulic head distribution within a single unit cell with periodic boundary conditions [*Kitanidis*, 1992; *Dykaar and Kitanidis*, 1992]:

$$\phi(L_1, x_2) = \phi(0, x_2) - JL_1 \tag{17}$$

$$\phi(x_1, L_2) = \phi(x_1, 0) \tag{18}$$

Because the fields of log-hydraulic conductivity $Y(\mathbf{x})$ and the hydraulic head fluctuations $\phi'(\mathbf{x})$ are periodic, the fields of specific discharge and seepage velocity $\mathbf{v}$ are also periodic and thus fully described by the distribution within a single cell. In our simulations, the flow field is evaluated by a standard cell-centered Finite Volume formulation for each realization, accounting for the periodic boundary conditions, equations (17) and (18). The linear system of equations is solved by a conjugate gradient solver with algebraic multigrid preconditioning [*Ruge and Stüben*, 1987].

[28] Transport is solved by the particle-tracking random-walk method using the semianalytical approach of *Pollock* [1988] for the advective displacement. In each realization, a pair of particles is introduced at the center of each Finite-Volume cell and tracked through the periodic domain over a dimensionless time period $tK_gJ/(\theta L_1)$ of unity. Particles leaving the unit cell at a boundary enter another unit cell

Table 2. Log Conductivity and Local Dispersion Parameters Used in the Simulations

Number	Log Conductivity Field	Local Dispersion	Remarks
1	highly resolved	$\mathbf{D}$	yields numerical solution of $\mathbf{D}^*(t)$ and $\mathbf{D}^e(t)$
2	kriged	$\mathbf{D}$	yields numerical solution of $\mathbf{D}^*(t) - \mathbf{D}^*_c(t)$ and $\mathbf{D}^e(t) - \mathbf{D}_c$
3	kriged	max $(\mathbf{D} + \mathbf{D}^*_c(t), \mathbf{0})$	full correction macrodispersion tensor
4	kriged	$\mathbf{D} + \mathbf{D}^e_c(t, \mathbf{0})$	full correction effective dispersion tensor
5	kriged	$\mathbf{D} + \mathbf{D}^e_{c,\ell}(t, \mathbf{0})$	only longitudinal correction of effective dispersion
6	kriged	$\mathbf{D} + \mathbf{D}^e_{c,t}(t, \mathbf{0})$	only transverse correction of effective dispersion

with identical flow field. That is, we can reintroduce the particle at the opposite side of the unit cell and add/subtract the corresponding length L_i to/from the particle's position within the unit cell to gain its global position. Altogether 50 million particles are tracked on average once through the unit cell. The one-particle variance of displacement $\langle \mathbf{X}'\mathbf{X}'^T \rangle (t)$ at time t is evaluated by:

$$\langle \mathbf{X}'\mathbf{X}'^T \rangle(t) = \frac{1}{2n_r n_c} \left(\sum_{j=1}^{n_r} \sum_{k=1}^{n_c} \mathbf{X}_1(j,k,t)\mathbf{X}_1^T(j,k,t) + \mathbf{X}_2(j,k,t) \cdot \mathbf{X}_2^T(j,k,t) \right) - \frac{1}{4n_r^2 n_c^2} \cdot \left(\sum_{j=1}^{n_r} \sum_{k=1}^{n_c} \mathbf{X}_1(j,k,t) + \mathbf{X}_2(j,k,t) \right) \cdot \left(\sum_{j=1}^{n_r} \sum_{k=1}^{n_c} \mathbf{X}_1^T(j,k,t) + \mathbf{X}_2^T(j,k,t) \right) \quad (19)$$

in which n_r is the number of realizations, n_c is the number of Finite-Volume cells, $\mathbf{X}_1(j, k, t)$ is the displacement at time t of particle 1 starting at time zero in the center of cell k in realization j, and $\mathbf{X}_2(j, k, t)$ is the same quantity for particle 2. The displacement is the actual position of the particle at time t minus the coordinates of the starting point. The two-particle variogram of displacement $\mathbf{\Gamma}_{\mathbf{X}\mathbf{X}^T}(t)$ is given by:

$$\mathbf{\Gamma}_{\mathbf{X}\mathbf{X}^T}(t) \equiv \langle \mathbf{X}'\mathbf{X}'^T \rangle(t) - \langle \mathbf{X}'_1\mathbf{X}'^T_2 \rangle(t) = \frac{1}{2n_r n_c} \left(\sum_{j=1}^{n_r} \sum_{k=1}^{n_c} (\mathbf{X}_1(j,k,t) - \mathbf{X}_2(j,k,t)) \cdot \left(\mathbf{X}_1^T(j,k,t) - \mathbf{X}_2^T(j,k,t)\right) \right) \quad (20)$$

The one-particle variance of displacement $\langle \mathbf{X}'\mathbf{X}'^T \rangle$ (t) and the two-particle variogram of displacement $\mathbf{\Gamma}_{\mathbf{X}\mathbf{X}^T}(t)$ are evaluated at discrete times with a dimensionless increment $\Delta t K_g J/(\theta \Delta x_1)$ of unity. Subsequently, the macrodispersion and effective dispersion tensors are calculated by numerical differentiation with respect to time:

$$\mathbf{D}^*(t) = \frac{1}{2} \frac{\langle \mathbf{X}'\mathbf{X}'^T \rangle(t + \Delta t) - \langle \mathbf{X}'\mathbf{X}'^T \rangle(t)}{\Delta t} \quad (21)$$

$$\mathbf{D}^e(t, \mathbf{0}) = \frac{1}{2} \frac{\mathbf{\Gamma}_{\mathbf{X}\mathbf{X}^T}(t + \Delta t) - \mathbf{\Gamma}_{\mathbf{X}\mathbf{X}^T}(t)}{\Delta t} \quad (22)$$

[29] We apply the particle-tracking random walk method to both the highly resolved and the kriged log conductivity fields and calculate the macrodispersion and effective dispersion tensors, $\mathbf{D}^*(t)$ and $\mathbf{D}^e(t, \mathbf{0})$, according to equations (21) and (22). Using the true local dispersion coefficient in the simulations, these calculations allow a comparison to the theoretical values of all dispersion coefficients mentioned. In subsequent calculations, we increase the local dispersion in the calculations on the kriged fields attempting to meet the same macrodispersion or effective dispersion values as observed on the highly resolved grid. Table 2 summarizes the conductivity and dispersion parameters in the various simulations.

4.2. Comparison Between Numerical and Analytical Results

[30] Figure 3 shows the principal components of the macrodispersion and effective dispersion tensors, $\mathbf{D}^*(t)$ and $\mathbf{D}^e(t, \mathbf{0})$, as evaluated by the particle-tracking random-walk method and the analytical expressions from first-order analysis, equations (11) and (13). The agreement between numerical and analytical results is very good for the macrodispersion coefficients. Due to the periodicity of the domain, the longitudinal macrodispersion coefficient D^*_{11} increases shortly before the center of the plume is advected once through the unit cell whereas the transverse macrodispersion coefficient D^*_{22} becomes negative at this time. This behavior deviates from that expected in stationary media. However, it is anticipated in periodic media because of the perfect correlation of log conductivity at the longitudinal separation distance $h_1 = L_1$. In the numerical simulation, the negative transverse macrodispersion is less pronounced and appears earlier than in the analytical solution.

[31] The discrepancy between numerical and analytical results is higher for the effective dispersion coefficients with point-like injection $\mathbf{D}^e(t, \mathbf{0})$ than for macrodispersion. In comparison to the results from particle tracking, the first-order theory underestimates the longitudinal effective dispersion coefficient systematically by about 20 percent. The underestimation by first-order analysis is, in relative terms, even stronger for the transverse effective dispersion coefficient. These results indicate that higher-order effects may become important in the evolution of two-particle moments in advection-dominated transport even for fairly small values of the log conductivity variance.

[32] We repeat the flow calculation and particle-tracking procedure on the kriged log conductivity fields and evaluate the corresponding macrodispersion and effective dispersion coefficients. The difference between these coefficients and the corresponding ones retrieved by transport calculations on the highly resolved fields are the correction macrodispersion and correction effective dispersion tensors, $\mathbf{D}^*_c(t)$ and $\mathbf{D}^e_c(t, \mathbf{0})$. Figure 4 shows the principal components

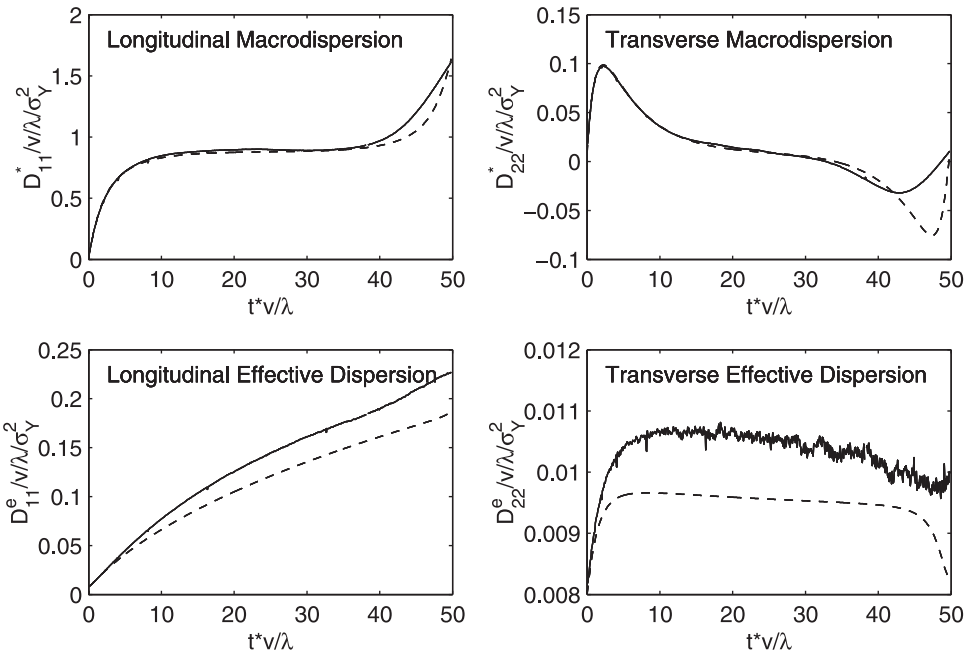

Figure 3. Dispersive quantities using the highly resolved grid. Solid line shows numerical simulation; dashed line shows analytical result.

of $\mathbf{D}^*_c(t)$ and $\mathbf{D}^e_c(t, \mathbf{0})$, as evaluated by the particle-tracking random-walk method in comparison to those derived from substituting the spatially averaged conditional covariance of log conductivity $\bar{R}_c(\mathbf{h})$ into equations (11) and (13). As in the case of the unconditional macrodispersion, shown in Figure 3, the agreement between the numerical and analytical results is excellent for macrodispersion, the only exception being the transverse correction macrodispersion at the time when the theory requires significant negative values because of periodicity. Since large-scale structures are covered well by the kriging estimate, the integral scale of the conditional covariance of log conductivity $\bar{R}_c(\mathbf{h})$ is smaller than that of the unconditional covariance $R_{YY}(\mathbf{h})$, and the correction macrodispersion coefficients reach their asymptotic values faster than the original macrodispersion coefficients. In the example, the amount of macrodispersion lost due to smoothing is about one fifth of the true value.

[33] The comparison between analytical and numerical results of the correction effective dispersion shown in

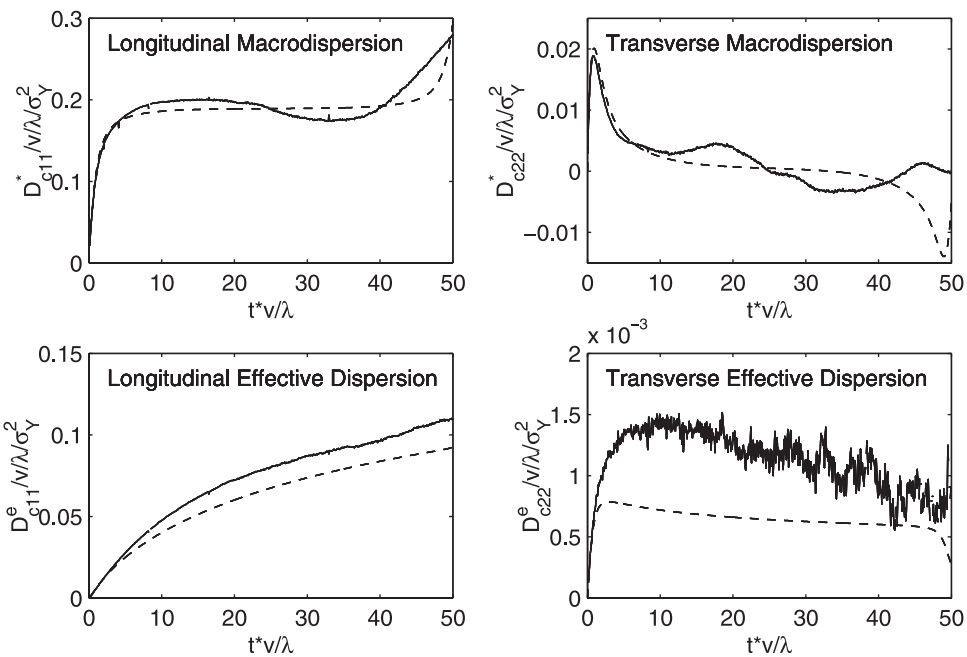

Figure 4. Components of the correction dispersion coefficient. Solid line shows numerical simulation; dashed line shows analytical result.

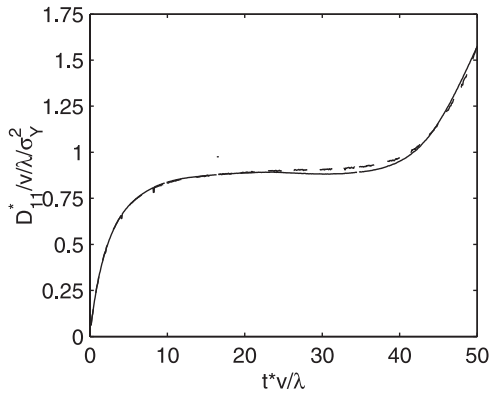

Figure 5. Longitudinal macrodispersion coefficient. Solid line shows highly resolved conductivity field; dashed line shows kriged conductivity field using increased local dispersion tensor.

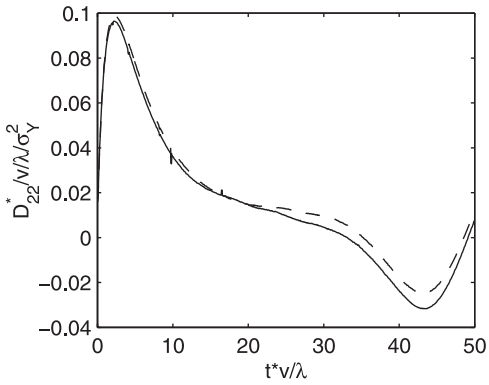

Figure 6. Transverse macrodispersion coefficient. Solid line shows highly resolved conductivity field; dashed line shows kriged conductivity field using increased local dispersion tensor.

Figure 4 is similar to the highly resolved case shown in Figure 3. A systematic underestimation by the analytical approach can be observed, but the trend is covered well. For the travel times considered, the smoothing of the grids has a stronger effect on effective dispersion than on macrodispersion. The amount of longitudinal effective dispersion lost due to smoothing is almost one half of the true value. Effective dispersion is governed by local dispersion making the plume sample increasing scales of heterogeneity. At earlier times, smaller scales of heterogeneity are sampled, and these are more affected by using a kriged rather than the highly resolved log conductivity field. In general, this holds for both longitudinal and transverse effective dispersion. In the example given, however, the absolute values of transverse effective dispersion are only by one fourth larger than the local-scale value $D = 0.008\bar{v}\lambda\sigma_Y^2$ so that the underestimation due to smoothing the grid is not that relevant.

4.3. Increasing the Local Dispersion Coefficients

[34] We repeat the particle-tracking random-walk calculations on the kriged fields with increased local dispersion coefficients. We add the analytical expressions of the correction dispersion tensors, $\mathbf{D}_c^*(t)$ and $\mathbf{D}_c^e(t, \mathbf{0})$, or directional components of them, to the true local dispersion tensor. By adding $\mathbf{D}_c^*(t)$, we expect accurate macrodispersion in the calculations on the interpolated fields, whereas adding $\mathbf{D}_c^e(t, \mathbf{0})$ should yield correct effective dispersion. Due to periodicity, as illustrated in Figure 4, the transverse correction macrodispersion coefficient does have negative values when the mean travel distance approaches the length of the unit cell. At times when $D_t + D_{t,c}^*(t) < 0$, the coefficient used in the calculations is set to zero. Table 2 gives an overview over all calculations.

[35] Figures 5 and 6 show the comparison between the macrodispersion coefficients as evaluated numerically on the highly resolved log conductivity field using the true local dispersion tensor $\mathbf{D}$ and on the kriged log conductivity field using $\max(\mathbf{D} + \mathbf{D}_c^*(t), \mathbf{0})$ as local dispersion tensor. For longitudinal macrodispersion, shown in Figure 5, the agreement is almost perfect. For transverse macrodispersion, shown in Figure 6, the agreement is very good at times when the transverse correction macrodispersion coefficient $D_{t,c}^*(t)$ is positive. At times when local transverse dispersion must be set to zero, the correction approach yields too high values of transverse macrodispersion. It should be noted, however, that negative values of transverse macrodispersion are an artifact of periodicity. In a stationary field, the transverse macrodispersion coefficients are always positive. Model results not plotted in the figures show that, by using $\max(\mathbf{D} + \mathbf{D}_c^*(t), \mathbf{0})$ as local dispersion tensor on the kriged log conductivity field, we strongly overestimate effective dispersion. This behavior is anticipated by $\mathbf{D}_c^*(t)$ being much larger than $\mathbf{D}_c^e(t, \mathbf{0})$.

[36] Figures 7 and 8 show the comparison between the effective dispersion coefficient as evaluated numerically on the highly resolved log conductivity field using the true local dispersion tensor $\mathbf{D}$ and on the kriged log conductivity field adding $\mathbf{D}_c^e(t, \mathbf{0})$ or components of it to the true local dispersion tensor. As shown in Figure 7, adding either the full correction effective dispersion tensor $\mathbf{D}_c^e(t, \mathbf{0})$ or only its longitudinal component to the true local dispersion tensor $\mathbf{D}$, yields excellent results of longitudinal effective dispersion. Adding only the transverse component of $\mathbf{D}_c^e(t, \mathbf{0})$, on the contrary, leads to an underestimation of longitudinal mixing. In the application given, apparently, the values of

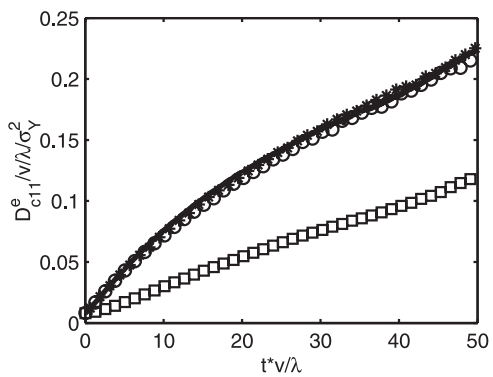

Figure 7. Longitudinal effective dispersion coefficient for point-like injection. Solid line shows highly resolved conductivity field; markers show kriged conductivity field using increased local dispersion tensor. Circles, longitudinal correction; squares, transverse correction; asterisks, longitudinal and transverse correction.

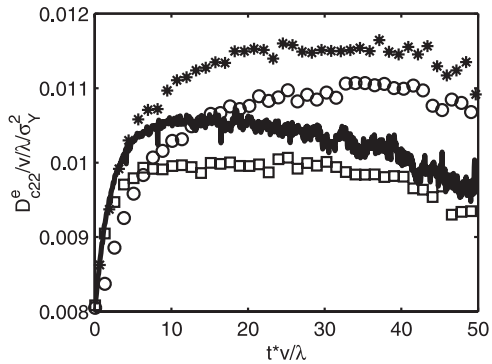

Figure 8. Transverse effective dispersion coefficient for point-like injection. Solid line shows highly resolved conductivity field; markers show kriged conductivity field using increased local dispersion tensor. Circles, longitudinal correction; squares, transverse correction; asterisks, longitudinal and transverse correction.

transverse correction effective dispersion are too small to have a major impact on longitudinal mixing. For transverse effective dispersion, as shown in Figure 8, the situation is somewhat more complicated. Adding the longitudinal component of $\mathbf{D}^e_c(t, \mathbf{0})$ to $\mathbf{D}$ leads to an increase in transverse mixing, although delayed. Adding the transverse component of $\mathbf{D}^e_c(t, \mathbf{0})$ to $\mathbf{D}$ gives the correct rate of change of transverse effective dispersion at early times. The values, however, do not reach the correct maximum. Finally, adding the full correction effective dispersion tensor $\mathbf{D}^e_c(t, \mathbf{0})$ to the local one causes slight overestimation of transverse mixing. However, keeping in mind that, with the given variability, the overall increase of transverse effective dispersion is smaller than the true local value, using either correction approach may be considered satisfactory. This may be different for fields with higher variance of log conductivity.

[37] Model results not plotted in the figures show that, by using $\mathbf{D} + \mathbf{D}^e_c(t)$ as local dispersion tensor on the kriged log conductivity field, we underestimate macrodispersion. We can quantify the lack of macrodispersion by $\mathbf{D}^*_c(t) - \mathbf{D}^e_c(t)$. In applications requiring the correct approximation of both macrodispersion and effective dispersion, such as in the prediction of breakthrough curves in mixing-controlled reactive transport, we suggest to perform the calculations on the smoothed log conductivity field using the sum of correction effective dispersion tensor and the true local dispersion tensor. This would guarantee a correct mass balance of the reacting compounds. Subsequently, the resulting breakthrough curves may be corrected for the lack in the second central moments in a parameterized form.

5. Summary and Conclusions

[38] The main results of the study may be summarized as follows.

1. Geostatistical interpolation of log conductivity measurements leads to the best linear unbiased estimate (BLUE) of the log conductivity distribution. The interpolated distribution is too smooth. The lack of variability can be approximated by the conditional covariance which is a result of the kriging procedure and does not depend on the actual measured values.

2. The conditional covariance is nonstationary. For measurements on a regular, rather dense grid we may remove the nonstationarity by taking spatial averages.

3. The spatially averaged conditional covariance of log conductivity can be substituted into the analytical expressions for macrodispersion and effective dispersion from first-order theory. The resulting correction dispersion tensors quantify the lack of dispersion when performing the calculations on the kriged rather than the fully resolved grid.

4. By adding the analytical expressions for the correction macrodispersion and correction effective dispersion tensors, respectively, to the true local dispersion tensor in calculations on the interpolated log conductivity fields, we get plumes with either the correct overall spreading or mixing behavior.

5. Our approach averages over all possible starting points. If we wanted to quantify the uncertainty in tagging a particle in the kriged field starting at a definite point, we had to follow a rigorous nonstationary approach such as that of *Indelman and Rubin* [1996] for advective transport, because the mean trajectory on the kriged field depends on the location of the injection point. That is, we expect that our approach is applicable only to wide plumes.

6. It is important to distinguish between macrodispersion and effective dispersion. In our approach, we cannot meet both. We believe, however, that quantifying the lack of macrodispersion when meeting the correct mixing behavior will be sufficient in many applications.

[39] *Cirpka* [2002] has applied the approach successfully to mixing-controlled multicomponent reactive transport.

Appendix A: Semianalytical Approach for the Spatially Averaged Conditional Covariance

[40] We derive $\bar{R}_c(\mathbf{h})$ for the 2-D exponential model in a periodic domain. Measurements are taken on a regular grid (denoted by index t) of $m_x \times m_y = m$ locations with spacing spacings d_{t_x} and d_{t_y}. Interpolations are performed on a highly resolved grid (denoted by index s) with $n_x \times n_y = n$ points and spacings d_{s_x} and d_{s_y}. The unconditional and conditional covariance matrices $R(\mathbf{x}_1, \mathbf{x}_2)$ and $R_c(\mathbf{x}_1, \mathbf{x}_2)$ relating all points on the fine grid to each other are denoted by the $n \times n$ matrices $\mathbf{R}_{ss}$ and $\mathbf{R}_{c_{ss}}$, the unconditional covariance matrices $R(\mathbf{x}_1, \mathbf{x}_2)$ on the grid of observations is denoted by the $m \times m$ matrix $\mathbf{R}_{tt}$, the discretized separation-related covariance $R(\mathbf{h})$ on the fine grid by $\mathbf{R}_s$ ($1 \times n$) and on the grid of observations by $\mathbf{R}_t$ ($1 \times m$), and the spatially averaged conditional covariance matrix $\bar{R}_c(\mathbf{h})$ on the fine grid by $\mathbf{R}_{c_s}$ ($1 \times n$). λ_x and λ_y are the correlation lengths in x- and y direction L_x and L_y the domain lengths, and $\mathbf{u}$ and $\mathbf{U}$ are vectors and matrices with unity entries. We require $L_x \gg \lambda_x$ and $L_y \gg \lambda_y$ to avoid overlapping of covariance functions. A $1 \times n$ matrix does not imply a 1-D domain, but arranging all points in a vector-shaped data array. Equation (8) is in this notation:

$$\mathbf{R}_{c_{ss}} = \mathbf{R}_{ss} - \mathbf{R}_{st}\mathbf{P}_{tt}\mathbf{R}_{ts} - \mathbf{u}_s P_\beta \mathbf{u}_s^T - \mathbf{u}_s \mathbf{p}_{\beta t}\mathbf{R}_{ts} - \mathbf{R}_{st}\mathbf{p}_{t\beta}\mathbf{u}_s^T \quad \text{(A1)}$$

See equation (9) for explanation of the P-coefficients. $\mathbf{R}_{st} = \mathbf{R}_{ts}^T$ is the $n \times m$ matrix of the covariance relating all points on the fine grid to all observation points. Applying the rules for

the inverse of a partitioned matrix [see, e.g., *Schweppe*, 1973], we obtain

$$\mathbf{P}_{tt} = \mathbf{R}_{tt}^{-1} + \mathbf{R}_{tt}^{-1}\mathbf{u}_t P_\beta \mathbf{u}_t^T \mathbf{R}_{tt}^{-1} \tag{A2}$$

$$\mathbf{p}_{\beta t} = -P_\beta \mathbf{u}_t^T \mathbf{R}_{tt}^{-1} = \mathbf{p}_{t\beta}^T \tag{A3}$$

$$P_\beta = \left(0 - \mathbf{u}_t^T \mathbf{R}_{tt}^{-1}\mathbf{u}_t\right)^{-1} \tag{A4}$$

For regular periodic observation grids, $\mathbf{R}_{tt} = \mathbf{R}_{tt}^T$, $\mathbf{R}_{tt}^{-1} = (\mathbf{R}_{tt}^{-1})^T$, and all sums of rows and columns are identical. Multiplication $\mathbf{Au}$ or $\mathbf{u}^T\mathbf{A}$ is the summation of rows or columns, so that $P_\beta = \bar{\mathbf{R}}_{tt}$, the mean of $(\mathbf{R}_{tt})_{jk}$, as $\mathbf{R}_{tt}$ can be shown to be the sum of all $(\mathbf{R}_{tt}^{-1})_{jk}$. Then:

$$\mathbf{P}_{tt} = \mathbf{R}_{tt}^{-1} - m^2(\bar{\mathbf{R}}_{tt})^{-1}\mathbf{U}_{tt} \tag{A5}$$

$$\mathbf{p}_{\beta t} = \frac{1}{m}\mathbf{u}_t^T = \mathbf{p}_{t\beta}^T \tag{A6}$$

$$\begin{aligned}\mathbf{R}_{c_{ss}} = \mathbf{R}_{ss} - \mathbf{R}_{st}\left(\mathbf{R}_{tt}^{-1} - m^2\left(\overline{\mathbf{R}}_{tt}\right)^{-1}\mathbf{U}_{tt}\right)\mathbf{R}_{ts} + \overline{\mathbf{R}}_{tt}\mathbf{u}_s\mathbf{u}_t^T \\ - \frac{1}{m}\mathbf{u}_s\mathbf{u}_t^T\mathbf{R}_{ts} - \frac{1}{m}\mathbf{R}_{st}\mathbf{u}_t\mathbf{u}_s^T\end{aligned} \tag{A7}$$

We average over all starting points $\mathbf{x}_1$ keeping the separation vector $\mathbf{h} = \mathbf{x}_2 - \mathbf{x}_1$ constant:

$$\begin{aligned}\overline{\mathbf{R}_{c_{ss}}}^{x_1} = \overline{\mathbf{R}}_{ss} - \overline{\mathbf{R}_{st}\left(\mathbf{R}_{tt}^{-1} - m^2\left(\overline{\mathbf{R}}_{tt}\right)^{-1}\mathbf{U}_{tt}\right)\mathbf{R}_{ts}}^{x_1} + \overline{\overline{\mathbf{R}}_{tt}\mathbf{u}_s\mathbf{u}_t^T}^{x_1} \\ - \overline{\frac{1}{m}\mathbf{u}_s\mathbf{u}_t^T\mathbf{R}_{ts}}^{x_1} - \overline{\frac{1}{m}\mathbf{R}_{st}\mathbf{u}_t\mathbf{u}_s^T}^{x_1}\end{aligned} \tag{A8}$$

in which the last three terms represent the mean of $\mathbf{R}_t$ and $\mathbf{R}_s$. We define the $n \times n$ permutation matrix $\mathbf{I}_s(\mathbf{h})$: $\mathbf{R}_s(\mathbf{h_0})\mathbf{I}_s(\mathbf{h}) = \mathbf{R}_s(\mathbf{h} + \mathbf{h_0})$, and rearrange:

$$\bar{\mathbf{R}}_{c_s}(\mathbf{h}) = \mathbf{R}_s - \sum_{j=k}^{m} \overline{\mathbf{R}_{st}\mathbf{R}_{ts}}^{x_1}\mathbf{I}_s\left(\mathbf{h}_j - \mathbf{h}_k\right)\left(\mathbf{P}_{tt}\right)_{j,k} + \overline{\mathbf{R}}_t\mathbf{u}_s - 2\overline{\mathbf{R}}_s\mathbf{u}_s \tag{A9}$$

where $\mathbf{h}_j$ is the distance of the jth observation point from the observation point at the origin, and k is arbitrary. For periodic domains we enforce $\overline{\mathbf{R}}_t = \overline{\mathbf{R}}_s = 0$ by subtracting the mean value from all entries. When inverting $\mathbf{R}_{tt}$, we do not apply this correction to avoid a bad condition of the matrix. No error results, as $\mathbf{P}_{tt}$ includes a correction for $\overline{\mathbf{R}}_{tt}$.

[41] In equation (A9), the only term of size $n \times n$ is $\mathbf{R}_{st}\mathbf{R}_{ts}$ prior to spatial averaging. Due to the averaging, we may replace $\mathbf{R}_{st}$ and $\mathbf{R}_{ts}$ by $m\mathbf{R}_s$, and execute summation first. Then we replace summation by integration:

$$\begin{aligned}\overline{\mathbf{R}_{st}\mathbf{R}_{ts}}^{x_1} &= \frac{m_x m_y}{n_x n_y}\sigma^4 \\ &\cdot \sum_{j=1}^{n_x}\sum_{k=1}^{n_y} \exp\left(-\sqrt{\left(\frac{h_{x_j}}{\lambda_x} + j\frac{d_{s_x}}{\lambda_x}\right)^2 + \left(\frac{h_{x_k}}{\lambda_x} + k\frac{d_{s_y}}{\lambda_y}\right)^2}\right) \\ &\cdot \exp\left(-\sqrt{\left(j\frac{d_{s_x}}{\lambda_x}\right)^2\left(+k\frac{d_{s_y}}{\lambda_y}\right)^2}\right) \\ &= \sigma^4\frac{\lambda_x\lambda_y}{d_{s_x}d_{s_y}}\int_{-\infty}^{+\infty}\int \exp\left(-\sqrt{\left(\frac{h_x}{\lambda_x} + x\right)^2 + \left(\frac{h_y}{\lambda_y} + y\right)^2}\right. \\ &\left. - \sqrt{x^2 + y^2}\right)dx\,dy\end{aligned} \tag{A10}$$

which is the volume under a surface with elliptic isocontours. The infinite integral is numerically exact for $L_x \gg \lambda_x$ and $L_y \gg \lambda_y$ and small d_{s_x} and d_{s_y}. If an integrand has isocontours $z = f(x(r), y(r))$ with enclosed area $A(r)$, then:

$$\int\int f(x,y)dxdy = \int z(r)\frac{dA}{dr}dr \tag{A11}$$

As in equation (A10) we integrate from $-\infty$ to $+\infty$, we may rotate and offset to obtain unit ellipses with apexes ($\pm a$, 0) and (0, $\pm b$), $|a| \geq |b|$, focal points ($\pm c$, 0), $c^2 = a^2 - b^2$, and $A = \pi ab$:

$$\frac{x^2}{a^2} + \frac{y^2}{b^2} = 1, \qquad c = \frac{1}{2}\sqrt{\frac{h_x^2}{\lambda_x^2} + \frac{h_y^2}{\lambda_y^2}} \tag{A12}$$

and therefore:

$$\begin{aligned}\overline{\mathbf{R}_{st}\mathbf{R}_{ts}}^{x_1} &= \sigma^4\frac{\lambda_x\lambda_y}{d_x d_y} \\ &\cdot \int_{-\infty}^{+\infty}\int \exp\left(-\sqrt{(x+c)^2+y^2} - \sqrt{(x-c)^2+y^2}\right)dx\,dy \\ &= \sigma^4\frac{\lambda_x\lambda_y}{d_x d_y}\pi\int_0^{\infty}\exp\left(-2\sqrt{b^2+c^2}\right)\frac{2b^2+c^2}{\sqrt{b^2+c^2}}db\end{aligned} \tag{A13}$$

This integral can be evaluated numerically and converges rapidly as the integrand exponentially approaches zero for increasing b. Substituting $\overline{\mathbf{R}_{st}\mathbf{R}_{ts}}^{x_1}$ as retrieved from equation (A13) into equation (A9) yields the spatially averaged covariance function $\bar{R}_c(\mathbf{h})$ discretized on the fine grid. The extension to 3-D is straightforward by using ellipsoids instead of ellipses.

[42] **Acknowledgments.** This study has been funded by the Deutsche Forschungsgemeinschaft under the grant Ci 26/3-2 "Experimental and Numerical Studies on Mixing of Reactive Compounds in Groundwater". We want to thank Sabine Attinger and two anonymous reviewers for their constructive comments.

References

Attinger, S., M. Dentz, H. Kinzelbach, and W. Kinzelbach, Temporal behaviour of a solute cloud in a chemically heterogeneous porous medium, *J. Fluid Mech.*, *386*, 77–104, 1999.

Bakr, A. A., L. W. Gelhar, A. L. Gutjahr, and J. R. MacMillan, Stochastic analysis of spatial variability in subsurface flows, 1, Comparison of one- and three-dimensional flows, *Water Resour. Res.*, *14*(2), 263–271, 1978.

Cirpka, O. A., Choice of dispersion coefficients in reactive transport calculations on smoothed fields, *J. Contam. Hydrol.*, *58*(3–4), 261–282, 2002.

Dagan, G., Solute transport in heterogeneous porous formations, *J. Fluid Mech.*, *145*, 151–177, 1984.

Dagan, G., Time-dependent macrodispersion for solute transport in anisotropic heterogeneous aquifers, *Water Resour. Res.*, *24*(9), 1491–1500, 1988.

Dentz, M., H. Kinzelbach, S. Attinger, and W. Kinzelbach, Temporal behavior of a solute cloud in a heterogeneous porous medium, 1, Point-like injection, *Water Resour. Res.*, *36*(12), 3591–3604, 2000.

Dykaar, B. B., and P. K. Kitanidis, Determination of the effective hydraulic conductivity for heterogeneous porous media using a numerical spectral approach, 1, Method, *Water Resour. Res.*, *28*(4), 1155–1166, 1992.

Fiori, A., Finite Peclet extensions of Dagan's solutions to transport in anisotropic heterogeneous formations, *Water Resour. Res.*, *32*, 193–198, 1996.

Fiori, A., and G. Dagan, Concentration fluctuations in aquifer transport: A rigorous first-order solution and applications, *J. Contam. Hydrol.*, *45*(1–2), 139–163, 2000.

Gelhar, L. W., and C. L. Axness, Three-dimensional stochastic analysis of macrodispersion in aquifers, *Water Resour. Res.*, *19*(1), 161–180, 1983.

Indelman, P., and Y. Rubin, Solute transport in nonstationary velocity fields, *Water Resour. Res.*, *32*(5), 1259–1267, 1996.

Kitanidis, P. K., Prediction by the method of moments of transport in heterogeneous formations, *J. Hydrol.*, *102*(1–4), 453–473, 1988.

Kitanidis, P. K., Orthonormal residuals in geostatistics: Model criticism and parameter estimation, *Math. Geol.*, *23*(5), 741–758, 1991.

Kitanidis, P. K., Analysis of macrodispersion through volume-averaging: Moment equations, *Stochastic Hydrol. Hydraul.*, *6*, 5–25, 1992.

Kitanidis, P. K., Analytical expressions of conditional mean, covariance, and sample functions in geostatistics, *Stochastic Hydrol. Hydraul.*, *10*, 279–294, 1996.

McLaughlin, D., and L. R. Townley, A reassessment of the groundwater inverse problem, *Water Resour. Res.*, *32*(5), 1131–1161, 1996.

Neuman, S. P., C. L. Winter, and C. M. Newman, Stochastic theory of field-scale Fickian dispersion in anisotropic porous media, *Water Resour. Res.*, *23*(3), 453–466, 1987.

Pollock, D. W., Semianalytical computation of path lines for finite-difference models, *Ground Water*, *26*(6), 743–750, 1988.

Rajaram, H., and L. W. Gelhar, Plume scale-dependent dispersion in heterogeneous aquifers, 2, Eulerian analysis and three-dimensional aquifers, *Water Resour. Res.*, *29*(9), 3261–3276, 1993.

Rubin, Y., Prediction of tracer plume migration in disordered porous media by the method of conditional probabilities, *Water Resour. Res.*, *27*(6), 1291–1308, 1991.

Rubin, Y., A. Sun, R. Maxwell, and A. Bellin, The concept of block-effective macrodispersivity and a unified approach for grid-scale- and plume-scale-dependent transport, *J. Fluid Mech.*, *395*, 161–180, 1999.

Ruge, J., and K. Stüben, Algebraic multigrid (AMG), in *Multigrid Methods, Frontiers in Applied Mathematics*, vol. 3, edited by S. F. McCormick, pp. 73–130, Soc. for Ind. and Appl. Math., Philadelphia, Pa., 1987.

Schweppe, F. C., *Uncertain Dynamic Systems*, pp. 495–498, Prentice-Hall, Old Tappan, N. J., 1973.

Sun, A., and D. Zhang, Prediction of solute spreading during vertical infiltration in unsaturated, bounded heterogeneoeus media, *Water Resour. Res.*, *36*(3), 715–723, 2000.

Zimmerman, D. A., et al., A comparison of seven geostatistically based inverse approaches to estimate transmissivities for modeling advective transport by groundwater flow, *Water Resour. Res.*, *34*(6), 1373–1413, 1998.

O. A. Cirpka and W. Nowak, Institut für Wasserbau, Universität Stuttgart, Pfaffenwaldring 61, 70550 Stuttgart, Germany. (olaf.cirpka@iws.uni-stuttgart.de; wolfgang.nowak@iws.uni-stuttgart.de)